AAC Accepted Manuscript Posted Online 1 February 2021
Antimicrob Agents Chemother doi:10.1128/AAC.01539-20

Parasite-host dynamics throughout antimalarial drug development stages complicate the translation of parasite clearance

Running title: Parasite clearance in antimalarial drug development

AUTHORS: Lydia Burgert[1, 2], Sophie Zaloumis[3], Saber Dini[3], Louise Marquart [4], Pengxing Cao [5], Mohammed Cherkaoui[6], Nathalie Gobeau[6], James McCarthy[4], Julie A. Simpson[3], Jörg J. Möhrle[1, 2, 6], Melissa A. Penny*[1, 2]

AFFILIATIONS: [1] Swiss Tropical and Public Health Institute, Basel, Switzerland, [2] University of Basel, Basel, Switzerland, [3] Centre for Epidemiology and Biostatistics, Melbourne School of Population and Global Health, University of Melbourne, Melbourne, Australia, [4] QIMR Berghofer Medical Research Institute, Brisbane, Australia, [5] School of Mathematics and Statistics, University of Melbourne, Melbourne, Australia,[6] Medicines for Malaria Venture, Geneva, Switzerland

*Corresponding author: melissa.penny@unibas.ch

Email of other authors:
lydia.burgert@swisstph.ch
sophiez@unimelb.edu.au
saber.dini@unimelb.edu.au
Louise.Marquart@qimrberghofer.edu.au
pengxing.cao@unimelb.edu.au
cherkaouim@mmv.org
gobeaun@mmv.org
J.mccarthy@uq.edu.au
julieas@unimelb.edu.au
moehrlej@mmv.org

1. Abstract

Ensuring continued success against malaria depends on a pipeline of new antimalarials. Antimalarial drug development utilizes pre-clinical murine and experimental human malaria infection studies to evaluate drug efficacy. A sequential approach is typically adapted, with results from each stage, informing the design of the next stage of development. The validity of this approach depends on confidence that results from murine malarial studies predict the outcome of clinical trials in humans. Parasite clearance rates following treatment are key parameters of drug efficacy. To investigate the validity of forward predictions, we developed a suite of mathematical models to capture parasite growth and drug clearance along the drug development pathway and estimated parasite clearance rates. When comparing the three infection experiments, we identified different relationships of parasite clearance with dose, and different maximum parasite clearance rates: in *P. berghei*-NMRI mouse infections we estimated a maximum parasite clearance rate of 0.2 [1/h]; in *P. falciparum*-SCID mouse infections 0.05 [1/h]; while in human volunteer infection studies with *P. falciparum*, we found a maximum parasite clearance rate of 0.12 [1/h] and 0.18 [1/h] after treatment with OZ439 and MMV048, respectively. Sensitivity analysis revealed that host-parasite driven processes account for up to 25% of variance in parasite clearance for medium-high doses of antimalarials. Although there are limitations in translating parasite clearance rates across these experiments, they provide insight into characterising key parameters of drug action and dose response, and assist in decision-making regarding dosage for further drug development.

Keywords: antimalarial drug development, translational medicine, parasite-host interactions, parasite clearance, within-host models

2. Introduction and Background

Recent progress in reducing malaria burden is threatened by emerging resistance against current first-line treatments and by sub-optimal adherence to existing treatment schedules. Development of new antimalarial treatments is therefore more urgent than ever (1). Requirements for new antimalarial treatment regimens are multi-facetted, spanning safety, efficacy, and dose optimization for all populations, including pregnant women, infants and children (2).

Before testing compounds *in vivo*, promising compounds are identified *in vitro*, and their parasiticidal efficacy is assessed in whole-cell or target-based assays (3). In pre-clinical stages, drug efficacy is often investigated using murine malarial infection. Historically, infection of normal mice with *P. berghei* was shown to be a useful experiment to measure crude drug efficacy and to select promising candidates (4). However, enzymatic differences between the human malaria parasite *P. falciparum* led to selection bias in candidate selection (5). More recently, the humanized mouse model of NOD $^{scidIL\text{-}2R'\ c\text{-}/\text{-}}$ (SCID) mice infected with *P. falciparum* has been shown to provide insights into efficacy against the human parasite *in vivo* (6–8) and further assists candidate selection. Early human efficacy studies via experimental infection of malaria-naïve individuals, termed volunteer infection studies (VIS)(9) or controlled human malaria infection (CHMI) studies, provide an opportunity to evaluate antimalarial activity in humans with low parasite burden in a controlled setting. These studies avoid the confounding factors of drug efficacy observed in clinical malaria cases such as acquired immunity, concomitant diseases and medication (10–12).

Drug efficacy indices, used to summarize drug effect over time, are key measures by which to evaluate the progression of drug candidates from the preclinical to clinical stages of the drug development pipeline. For malaria, pharmacodynamic/efficacy indices include: i) measurements of total or proportional parasite clearance such as the parasite clearance rate or parasite reduction ratio over 48 hours (PRR_{48}) (4); ii) drug exposure typically reported by indicative drug concentrations such as the minimum inhibitory concentration (MIC) (8); and iii) clinical endpoints such as adequate clinical and parasitological response (ACPR) (13). Parasite clearance measures are widely used in antimalarial drug development to guide compound selection (2), and are also reported in clinical studies in endemic areas as a measure of drug efficacy (14).

In a previous paper, we developed a suite of mathematical models of parasite growth and drug-parasite dynamics to investigate murine malaria infection and malaria drug experimental tests. Through extensive simulation of these models and comparison with data for several drugs, we found that the experimental systems and differences between the two murine malaria infections had appreciable effects on measured drug efficacy and treatment outcomes. More specifically, we found drug efficacy is influenced by host-parasite dynamics in *P. berghei*-NMRI mouse infection where resource limitation is caused by aggressive parasite growth, namely limitations of red blood cells (RBC)(15). In *P. falciparum*-SCID mouse infection, we found continued

injections of human RBCs has a noticeable impact on subsequent clearance patterns of uninfected and infected RBCs. We additionally identified mechanisms of observed recrudescence patterns after non-curative treatment that are not discernable from the experimental data nor captured by current modelling approaches of antimalarial drugs. These unknown mechanisms may include altered parasite maturation or dormancy and affect experimental measures of cure, thus limiting interpretations of curative dose for a particular drug (15).

In this study, we examined the ability of the parasite clearance after treatment estimated from murine experiments to translate to estimates in human studies. This analysis used data from studies of two antimalarials, MMV048 and OZ439 (artefenomel), in the *P.berghei* – NMRI mouse, in P. *falciparum* (strain 3D7) -SCID mouse and in *P.falciparum* (strain 3D7) -human infection experiments. Both compounds are part of the Medicines for Malaria Venture portfolio (https://www.mmv.org/research-development/mmv-supported-projects). OZ439 is a synthetic peroxide antimalarial candidate that is fast acting against all asexual erythrocytic parasite stages. It is currently being evaluated in combination with Ferroquine in phase II clinical studies(11, 16–18). MMV048 is a *Plasmodial* phosphatidylinositol 4-kinase (PI4K) inhibitor efficacious against liver erythrocytic parasite-life cycle stages currently in phase IIa (19–21).

We modelled parasite growth and clearance following two new antimalarial treatments in murine and human malarial infections (Figure 1a: model development and calibration). We included relevant and potentially important features of parasite growth, host, and drug dynamics in the models of all three testing systems following a comprehensive examination of their biological and experimental background. Through simulation and global sensitivity analysis of these models we explored and compared the estimates of parasite clearance for a range of dosing regimens, and parasite and host assumptions in all three systems (Fig. 1b). Through this analysis, we demonstrated which of the factors; host, parasite, host-parasite and drug dynamics, primarily determine the relationship between parasite clearance estimates across the antimalarial drug development pathway and assess implications for decision making in drug development.

3. Results

The design of the studies/experiments used to evaluate the candidate antimalarials (MMV048 and OZ439) in normal mice, SCID mice and human volunteers is described in Table 1 and Fig. 2 (left side of panels a-c). Mice were infected with around $2x10^7$ parasites or greater inocula resulting in progression to severe disease with high parasitemia of up to 60-80 % (*P. berghei*, parasitized mouse RBCs) and 15-20 % (*P. falciparum*, parasitized human RBCs) within a week of inoculation. By design, human volunteers do not progress to high parasitemia to avoid severe clinical illness (9). Volunteers reach parasitemia of around 10^4 p/mL (corresponding to 0.0002% under the assumption of $5x10^9$ RBCs/mL in male humans (22)) before treatment.

Parasite-host dynamics and experimental design influence treatment in murine malaria infection

In our previous work (15), we developed several mathematical models of parasite and drug dynamics in both *P. berghei*-NMRI and *P. falciparum*–SCID mice (Fig. 1a). The experimental system and mathematical models are described in Fig. 2, panels a and b, respectively. Using the parameter estimates from the original paper (for both parasite growth and PKPD models), we simulated the models of murine infection to compare their results with our VIS simulations below (Figure 1b). Here, we primarily compared parasite clearance after treatment across the three testing systems (Fig. 1b: Comparison of parasite clearance across experimental systems) as estimated from the models for a range of drug doses. We subsequently assessed the influence of experimental design and parasite-host system on parasite clearance throughout the antimalarial development pathway by sampling from the posterior distributions for VIS, and by sampling parameters from a log-normal distribution with 20% standard deviation for the murine models (Fig. 1b: sensitivity analysis).

In the two murine systems, several experimental and parasite-host traits were examined by including them in a suite of models (further details in Methods and Table S5) (15). From an experimental perspective, data availability and experimental design differ between the two murine infection systems. For example, in *P. berghei*-NMRI infection, the volume of blood sample needed for analysis and aggressive parasite growth limits the frequency of collection for measurements of parasitaemia. From the host perspective, we investigated and quantified adaptions of the host-system to increasing parasite burden. In *P. berghei*-NMRI infection, we included erythropoiesis (23, 24) or clearance patterns, as well as parasite adaptions such as parasite maturation (25) and target-RBC preferences (23) in our models to capture patterns of RBC availability and the occurrence of anemia (Fig. 2a). In *P. falciparum*–SCID infection experiments, continued injections of human erythrocytes hinder the occurrence of anemia and lead to an increase in the proportion of available human host-cells throughout the experiment (Fig. 2b). The injected human RBC volume of 4.55×10^9 RBCs every two to three days (corresponds to 46% of total mouse RBCs) leads to a high clearance of excess erythrocytes throughout the experiments, thus likely affecting measures of drug efficacy (6). Different

hypotheses regarding the influences on RBC clearance mechanisms were formalized in our models of *P. falciparum*-SCID mouse infection (Fig. 2b).

Using a maximum likelihood approach, we estimated the parameters of our parasite growth models by fitting them to the pooled experimental control data of untreated parasite growth. The fitted models were then combined with the PD models to analyze the influence of the parasite-host dynamics and experimental design on parasite clearance after treatment.

For MMV048, we captured the parasite clearance data after treatment by including a delayed parasite clearance of parasites damaged or killed by the drug, modelled by the clearance rate of dead parasites Cl_Y, in both murine hosts (Table S5- clearance PD model selection: Cl_Y range of 0.036 to 0.041 (1/h) in *P. berghei*-NMRI and Cl_Y range of 0.068 to 0.071 (1/h) in *P. falciparum*-SCID infection over all mechanistic parasite growth models). In contrast, for OZ439, we observed a delayed drug effect through a turnover (Table S5- turnover PD model selection: k_R range of 0.013-0.06 (1/h) in *P. berghei*-NMRI and k_R range of 0.013-0.016 (1/h) in *P. falciparum*-SCID infection over all mechanistic parasite growth models) (15). In both murine experimental systems, we found that assumptions on parasite-host dynamics result in differing estimates of parasite clearance times therefore influencing the evaluation of new compounds (see Fig. 4 in previous paper) (15).

Human volunteer infection studies exhibit large variation in observed parasite growth and clearance dynamics

We modelled parasite growth prior to treatment using data from 177 volunteers in 27 treatment cohorts in VIS conducted at Berghofer QIMR, Brisbane between 2012–2016 (26). These cohorts were part of 14 studies investigating new antimalarials in development and currently available antimalarials. Volunteers were infected with 1800–2800 infected RBCs and treated 7–9 days after inoculation (26).

Sampling frequency of human volunteers was much higher compared with murine experiments, however, the number of measurements above the lower limit of quantification (LLOQ, 111 p/mL) varied between cohorts and volunteers with a median of five quantifiable measurements (ranging from one to eight). These detailed data allowed us to capture features of the parasite life cycle, such as the characteristic oscillation in parasite densities. This phenomena is caused by periodical sequestration of late stage asexual parasites stages to the deep microvasculature of the host organs (27) and synchronicity in parasite growth determined by the distribution of parasite age in the inoculum (28).

The models of asexual parasite growth in in human volunteers are described in Fig 2c. We adapted a discrete time model (29) previously used to investigate antimalarial treatment (28), resistance against artemisinin combination therapy (30), and the impact of new antimalarial combinations (31). A set of difference equations (*model S-parasite stages*, Equation 7) describes the parasite inoculation, capturing its size and age distribution, and the subsequent mechanism of

intra-erythrocytic parasite development including ageing and parasite death. Based on analysis by Wockner et al., that quantified parasite growth behavior of *P. falciparum* (3D7) in VIS, the life-cycle length was set to 39 hours. (26) For comparison, we tested a second model that assumes exponential parasite growth (*model i*, Equation 10), summarizing parasite replication and death into one growth parameter. This model is commonly used to capture parasite growth and treatment effects in antimalarial drug development (8, 11).

We incorporated the models into a Bayesian hierarchical framework to estimate the posterior distributions of the model parameters from the VIS data. We investigated different levels of parameter variability, distinguishing between parasite and host dependent parameters by varying hierarchical parameter allocation in different parasite growth model specifications (Table S2, *models S1–S3*). *Model S3*, from here on referred to as *model S*, was selected based on the Watanabe-Akaike information criterion (WAIC) (Table S2). The parameters describing distribution of the initial parasite load (mean μ_{ipl} and standard deviation σ_{ipl}) and the intrinsic parasite multiplication factor, $r_{p,}$ were found to vary on a cohort level whereas the initial parasite load i_{pl} and parasite death rate due to host clearance δ_p vary between individuals (Figure S7). The population posterior predictions of the two parasite growth models (Fig. 3) begin on day 4 after inoculation, when quantifiable parasitemia measurements from the volunteers are first available (Fig. 2). We estimated a parasite multiplication factor *pmf*, of 17.0 (15.3–20.0) over one life cycle of 39 h (Equation 7). Identifiability issues of growth rate r_p were detected by the partial congruency of the marginal prior and posterior distributions (Figure S7). This means that data on parasite growth is not informative enough for estimating this parameter, similar to previous model analysis(32). For exponential growth *model i*, we estimated a *pmf* of 12.61 (11.2–14.2) over one parasite life cycle. Differences in the parasite growth rate r_p between individuals within cohorts, could not be linked to cohort or subject specific parameters for *model i* (Fig. S8).

Given our calibrated VIS parasite growth models, we incorporated PK models and modelled drug effects (pharmacodynamics) (Fig. 1a) to analyze single-dose treatment of 20 volunteers with MMV048 and 24 volunteers with OZ439 (Table S1). Drug concentrations after treatment were predicted using pharmacokinetic (PK) models (Equation S1and S2) and individual PK parameters specified (Supplementary File 1). We simulated individual PK profiles to exclude large variation in drug-concentration as an influencing factor in the following analysis. Drug concentration over time was described by a two-compartment model with zero-order absorption for MMV048 and a 2-compartment model with linear absorption for OZ439. In the following section, we explain the results for OZ439. The analysis of MMV048 is detailed in the Supplement, and any deviations are highlighted and discussed here.

We incorporated a direct effect of drug concentration on parasite death (Equation 8) and additionally tested for drug concentration induced retarded parasite growth (Equation 9) due to the reduced parasite growth observed after non-curative dosing with OZ439 and the shift in oscillation patterns to a longer period. This phenomenon was also previously described for

artemisinin derivatives (33). A comparison of drug action model based on WAIC and additional observations is included in Table S3.

We detected drug-concentration dependent prolongation of parasite stages after treatment with MMV048 and OZ439, meaning that at sufficiently high drug concentrations each life cycle stage can be prolonged by 26 min or 65 min respectively (Equation 13). Through description of individual treatment effects via subject-specific parameters of drug efficacy (Fig. S9-S12) we could capture individual parasite clearance and recrudescence curves after treatment with MMV048 (Figure S3 and S4) and OZ439 (Figure S5 and Figure S6) for all subjects.

Although the posterior predictions of recrudescence (Fig. 4) fit the data well, we note that informed mechanistic models, and inclusion of experimental recrudescence outcomes and cure are hindered by limited data on cure probability since each cohort only consisted of eight subjects. Additionally, insights into minimum parasite concentrations for cure are missing.

Parasite clearance is unlikely comparable across the preclinical and clinical development pathway

The parasite clearance after treatment was estimated from our model simulations for murine and human malaria infection (Fig. 1b) over a wide range of single doses of each drug. The range of doses and models facilitated comparison across preclinical and clinical stages. We chose seven doses per experimental system that capture realistic testing dose ranges. We simulated 1000 trials for each murine experiment with parameter estimates published in (15) (see Table S5 for an overview) and variability added between trials, with parameters fixed within one trial over all doses. In human-*P. falciparum* infections we simulated 100 trials with 20 subjects per dose and varied the parasite-dependent parameters between trials and the host-dependent parameters between subjects within a trial. The parameters of the PK models were fixed to population values for all model simulations to allow for adequate characterization of host-parasite dependent dynamics and variability. The simulation set-up is detailed in Table S4.

Fig. 5 compares parasite clearance calculated from simulation output after single dose treatment of OZ439 over the two murine and experimental human infection experiments. We find varying relationships of estimated parasite clearance with doses across the experimental systems. Median estimates of parasite clearance rates plateau around 0.2 [1/h] ($\log_{10}$ PRR_{48}: 4.17) in *P. berghei*-NMRI infection and 0.05 [1/h] ($\log_{10}$ PRR_{48}: 1.04) for *P. falciparum*-SCID infection. Analysis for MMV048 shows similar maximum clearance rates in murine infection (Fig. S13) and varying relationships with dose. In experimental *P. falciparum*-human infection the parasite clearance rate for OZ439 plateaus with *model S* around 0.12 [1/h] ($\log_{10}$ PRR_{48}: 2.50). The ranges of the predicted clearance time of *P. falciparum*-human infection between *model i* and *model S* are also reflected in the wider posterior predictive intervals of the former after treatment with OZ439 (Fig. 4).

Parasite clearance is influenced by varying parasite-host dynamics throughout the analyzed experiments of murine and human malaria infection. Despite the poor comparability across experimental systems, the parasite clearance predicted from mechanistic models within an experimental system are comparable, but with different levels of variation. Via a global sensitivity analysis, we thus identified which host-, parasite-, and drug-dynamics cause the highest variability in parasite clearance after treatment with MMV048 and OZ439. We first partitioned variability by classifying parameters by their influence and dependency on parasite-, host- or drug-concentrations. For example, the parameters of infection induced RBC clearance γ in murine malaria models are classified as host-parasite parameters since they are induced by parasite concentration and influence overall RBC concentration (Table 2). We then undertook a global sensitivity analysis of the models on simulated parasite clearance rates reducing computational time by using emulators and sobol-analysis, which calculates first order indices and total effect indices to evaluate individual and combined parameter contributions to the variance of parasite clearance rates (see Methods).

In general, we find in all experimental systems, that parasite clearance after treatment is most sensitive to drug action parameters, see Table 2. This is expected as we are measuring the effect of the drug in these systems. We also find that interactions of the drug action parameters (increased total effect over first-order effect) occur over all doses but decrease with increasing dose, evident in the convergence of first order and total effect values. However, in both the murine (Fig. 6b) and human *P. falciparum* (Fig. 6c) infections, we find at lower doses an increasing influence of both the host or parasite, or host-parasite parameters. This indicates a greater influence of the experimental system on measured parasite clearance. Even in medium-high dose ranges, drug unrelated parameters and their interactions account for up 25% of variance in parasite clearance. This is mainly caused by sensitivity towards maximum infection induced RBC clearance γ_{max} and parameter φ, which capture splenic/liver clearance and maximum infection induced RBC clearance γ_{max}. The exponential growth *model i* shows diminishing dependence on parasite replication rate r_p with increasing doses in *P. falciparum* – SCID infection.

Estimated treatment effects of experimental *P. falciparum*-human infection are sensitive to the maximum drug action parameter E_{max}, resulting in a large range of parasite clearance rate prediction throughout all doses. In the lower dose ranges of OZ439 treatment, the total effects of the age distribution parameters μ_{ipl} and σ_{ipl} of *model S* account for up to 50% of all variance (c). In contrast, throughout all regimens, parasite parameters have negligible influence on clearance for MMV048 (Fig. S14). The full set of individual parameter contributions in all experimental systems can be found in Supplementary File 2. The complete set of results for both drugs are shown in Fig. S14 and Fig. S15.

Antimicrobial Agents and Chemotherapy

4. Discussion

Our analysis of data from three unique experimental systems of drug action in *Plasmodium* infection: *P. berghei*-NMRI mouse infection, *P. falciparum*-SCID mouse infection and the human VIS, demonstrates a discrepancy in influencing parasite-, host- and drug-dynamics on parasite clearance between the pre-clinical and clinical antimalarial testing stages. This complicates the translation of results between these different experimental systems, which aim to collectively inform drug development. We initially intended to identify antimalarial drug efficacy indices that were reliable for translation. Although our analysis did not result in a unifying output, our insights into parasite-host dynamics across the preclinical murine and early clinical experimental infections in humans via the mathematical models provide a pathway to facilitate inference from the data. By describing the different experimental testing systems with data-calibrated mechanistic models, we used model predictions coupled with sensitivity analysis to identify factors significantly influencing experiments aimed to characterise drug efficacy. In addition to the drug and dose being tested, we identified differing magnitudes of host-parasite dynamics between the experimental systems as a driver of estimated parasite clearance rate.

By employing mechanistic models of parasite growth and drug effects in all three testing systems we found that several important dynamics affect translation of parasite clearance after treatment and likely other parasitological outcome measures between preclinical and clinical systems.

Firstly, as expected, our sensitivity analysis of parasite clearance revealed a high sensitivity to parameters of drug action in higher dose ranges in all three experimental systems. In contrast, we found a variation in overall sensitivity of parasite clearance to parasite-host dynamics in lower–medium dose ranges between the three experimental systems. In murine and human *P. falciparum* infection, parameters of parasite growth influenced parasite clearance after treatment with lower doses. Additionally, the occurrence of clearance mechanisms of excess RBCs in *P. falciparum*-SCID infection, could place additional constraints on parasite growth. Overall, the increased susceptibility to the experimental set-up of the SCID system limits direct translation and comparison of results between laboratories and highlights the need for strict experimental protocols (15, 34). Thus, to predict human equivalent doses by exploiting the value of the *P. falciparum*-SCID mouse system, additional information is required concerning the interplay of disease dynamics and the experimental background which could be quantified with our modelling approach. For *P. berghei*-NMRI infection data, estimation of the parasite clearance was less sensitive to parasite-host dynamics. However, the aggressive parasite growth in this experimental system might lead to host-cell limitations and therefore different growth dynamics compared to *P. falciparum* infection, challenging the translatability of drug efficacy measures. Although not investigated here, the uncertainties regarding clearance mechanisms may also hinder the investigation of drug-drug interactions. The testing of combination therapies relies on the ability to allocate contribution of each drug to effects on parasite clearance and to estimate potential drug interactions. *In vitro* experiments could prove to be valuable alternatives in

establishing formal descriptions of these interactions, which could thus be incorporated into mathematical models to predict the efficacy of combination (31).

Secondly, the sensitivity of parasite clearance measured at lower drug doses due to factors other than the drug raises questions for current approaches to determine concentration-effect relationships (Equation 12) that rely on information gained in lower-medium dose ranges to define the concentration with half-maximum effect (EC_{50}). Additionally, other common drug efficacy indices such as the minimum inhibitory drug concentration (MIC) are influenced by EC_{50} measures (Equation 16). We therefore recommend that inferences based on data gathered at low–medium doses across the preclinical and clinical stages of drug development are assessed by considering factors connected to experimental and host-parasite pairing. For example, in *P. falciparum*-SCID and *P. falciparum*-human infection experiments, the sensitivity of the dose-response relationship of data obtained at lower dose ranges should be investigated for each drug candidate to avoid bias in decision making. In experiments with a new compound where drug efficacy analysis reveals a substantial influence of parasite-host dynamics in lower dose ranges, these data should not be used to characterize the MIC for decision making.

Thirdly, our earlier work indicated that recrudescence and thus estimates of MIC are potentially influenced by additional parasite mechanisms including retarded parasite growth in *P. falciparum*-SCID experiments(15). Experiments explicitly aimed at observing recrudescence are considered highly informative in understanding the dose-response relationships in these experimental systems. However, utilizing these experiments for modelling proved that estimation or prediction of cure might be hindered by insufficient data on cure rates and curative doses in both murine and human malaria infection (Table 1). Thus, any analysis we could undertake on cure or recrudescence dynamics is driven by model assumptions and was therefore excluded from this analysis. We further excluded drug-concentration-dependent indices such as maximum concentration, time above a threshold concentration, and the area under the concentration time curve (AUC) because information on PK variability was missing, especially in murine experiments.

How well the parasite clearance rate could be quantified varied between the murine and human volunteer experimental infection data. In the murine malaria experiments, there is limited repeated blood sampling of each mouse and evaluating progression of infection was limited to measuring percentage of infected RBCs (Fig. 2). Additionally, the evidence for delayed clearance of dead parasites after treatment with MMV048 for both murine models (15) indicates that not only drug properties but also the host's ability to clear damaged/dead parasites are factors that are determining maximum clearance rate. In the VIS studies, drug treatment is typically administered at an earlier timepoint at a lower parasitemia, when volunteers are typically asymptomatic. Thus, data from these studies are collected at parasitemia levels up to five logs below those studied in endemic settings, a factor that may confound analysis of maximal parasite clearance.

We were able to compare drug efficacy as parasite clearance across the murine and human infection experiments, thereby measuring drug efficacy throughout antimalarial drug development, because the models formally considered experimental background (i.e. parasite-host combination and experimental procedures) as well as parasite dynamics. Across the mathematical models of parasite growth and treatment, we found that different levels of detail between the preclinical and clinical infection experiments were required to capture parasite growth and thus drug effect. In the mechanistic models of murine malaria infection, high-parasitemia and RBC clearance mechanisms necessitate inclusion of host-cell dynamics in the models. Parasite-host dynamics were influenced by either rapidly increasing parasite load (in the case of *P. berghei*-NMRI infection) or the experimental set-up including the continued human erythrocyte injections (in the case of *P. falciparum*-SCID infection). However, in VIS, explicit description of host-cell dynamics is not required due to lower parasite load and relatively short infection follow-up. This means, as patients are treated due to safety reasons when parasitaemia reaches a certain level, only few parasitaemia measurements during the initial growth phase are available and any effect of immune response on parasite dynamics is likely to be minimal, thus obviating the need to consider host responses in this model. Furthermore, due to the significant variability in parasite growth observed in the murine experiments, the parasite-growth models required calibrated parasite fitness parameters to capture differences between laboratories, as well as unmeasured differences in virulence of parasites transferred from donor mice in each experiment (ability of the parasite to infect new RBCS). Similarly, in VIS, parasite growth and synchronicity were dependent on the distribution of viable parasite life-cycle stages at inoculation, and models required estimates of these age distribution to recover observed oscillations.

For drug dynamics, we evaluated different pharmacodynamic models to capture the observed parasite clearance in murine and human infection. In murine experiments, delayed clearance of parasites damaged/killed by the drug and drug action through a turnover model were identified. Although *in vitro* experiments reported slight stage-specificity of OZ439(16), with an increased action against trophozoites and schizonts, data were too sparse in the VIS studies to provide a detailed analysis. We did not find evidence of delayed clearance of damaged or dead parasites (27) for the two compounds analyzed. However, this could change for other antimalarials depending on the mode of action, parasite load and data resolution.

Our estimated value of 17.0 (95% credible interval: 15.3-20.0) for the multiplication factor of the parasite after every 39-hour life cycle in *P. falciparum* (3D7) VIS is comparable to previous estimates of 16.4 (95% confidence interval: 15.1–17.8) (26) and 21.8 (95% credible interval:17.6–26.9, at a life cycle length of 42 h)(32) in VIS studies. The growth of parasitemia has been modelled using a variety of methods e.g. testing statistical models for quantification (26), assays for *in vivo* determination (35) and linking it to disease severity(36). However, we found a potential issue of statistical parameter identifiability for this rate where the intrinsic parasite multiplication rate exhibits weak identifiability and strong correlation with the parasite

death rate. Nevertheless, we decided to maintain both dynamics, an intrinsic growth rate and parasite death rate in the model instead of a net growth rate to capture differences between cohorts and individuals, and to highlight gaps in knowledge. In theory, the synchronous parasite growth in VIS could inform these two parameters if information on parasite age-distributions throughout the parasite life cycle were collected (37). However, this information was not available in the cohorts analyzed and in practice may be difficult to obtain. As parasite numbers after treatment are very low in VIS, the role of immunity for successful treatment is unknown from these studies. However, further analysis and modelling could combine information on parasite growth in clinical field trials in pre-exposed patients (38–40). Thus, potentially estimate the effect of the immune system on parasite growth to inform dosing recommendation.

The necessity for timely decisions regarding the progression of antimalarial compounds to the next experimental stages and design of future experiments might not allow for extensive analysis of data through mechanistic models for each drug. However, the mechanistic models developed and validated in the context of this study could serve as a tool to assess potential influences stemming from parasite-host dynamics and help to improve the experimental design of future experiments providing more depth than the analysis of experimental data alone.

Although drug efficacy data from these three discussed experimental systems allow the comparison of compounds within one *in vivo* experimental system, we are currently not able to translate parasite clearance measures between the systems. Furthermore, as assumptions on the mode of drug action potentially influence clearance patterns, either by data analysis or as predicted by the models, the comparison of compounds with different modes of action is complicated. Our analysis shows that there are different underlying parasite-host dynamics in each system that influence experimental analysis and thus drug efficacy evaluation (either by extrapolation or by models). Therefore, a reliable strategy to translate efficacy measures and produce insights from drug-parasite-host dynamics between the development stages has not yet been identified. Additionally, preclinical and early clinical testing of new compounds is expensive and time-consuming. This is especially true for antimalarials, as only combination therapies will be considered for Phase 3 clinical trials and future implementation. To identify appropriate combination therapies, combinations are currently tested in both, *P. falciparum*-SCID experiments (41) and *P. falciparum*-human infection in VIS (42). Therefore, we suggest that the value of current and new approaches in *in vitro* drug efficacy experiments should be revisited in antimalarial development.

In vitro experiments allow the possible identification of mode of drug action, stage specificity, and evaluation of parasite killing in dependence on the unbound drug-concentration without the influence of parasite-host dynamics. This can be achieved with current *in vitro* experiments (43, 44) or by developing new *in vitro* approaches.

Modelling and simulation strategies could thus be informed by more appropriate *in vitro* data unlike today, where large assumptions need to be made on parasite-host dynamics *in vivo*. The *in vitro* dose-response relationship could then be translated to predict human drug efficacy by taking into account parasite growth and clearance mechanisms in human VIS using mechanistic within-host parasite growth models. If validated, this approach could accelerate drug selection in antimalarial drug development by allowing a streamlined prediction of drug efficacy from *in vitro* experiments to humans, therefore reducing the need for substantial or complicated murine efficacy experiments. An investment in setting up new and appropriate *in vitro* experiments and analysis and/or model frameworks could therefore support the cost-efficient translation between experimental systems through efficient candidate selection and ability to inform early clinical dosing in real-life settings.

Acknowledgments

We acknowledge and thank our colleagues in the Swiss TPH Disease Dynamics unit, and our collaborators at MMV, QIMR-Berghofer and University of Melbourne. The work was funded by the Swiss National Science Foundation through SNSF Professorship of MAP (PP00P3_170702). Calculations were performed at sciCORE (http://scicore.unibas.ch/) scientific computing center at University of Basel. JA Simpson is supported by an Australian National Health and Medical Research Council Senior Research Fellowship (1104975).

5. Materials and Methods

Data, parasite growth and PKPD models in murine experiments

Models of murine malaria infection (Fig. 2) were calibrated to extensive parasite growth data and subsequent treatment with multiple antimalarial drugs (Table 1). Here, we briefly present the base structure (m*odel a*) of the ordinary differential equations for the murine malaria infection model as specified in (15) . Parasite growth within the host is described by ordinary differential equations capturing dynamics of uninfected murine host RBCs ($X_{m(murine)}$), infected RBCs (Y_{Xm}) and merozoites (M). RBC dynamics are incorporated with constant production υ [cells/h] and decay rate μ [1/h] and become infected through invasion with merozoites dependent on the infectivity parameter β [cells/mL h].

$$\frac{dX_m}{dt} = \nu - \mu_{X_m} X_m - \beta X_m M \qquad (1)$$

Infected RBCs (Y) burst after 1/ α hours to release r new Merozoites that die with rate δ [1/h]. The aging of the parasite throughout the parasite-life cycle is incorporated via n transit compartments.

$$\frac{DY_{Xm,1}}{dt} = \beta X_m M - \alpha Y_{Xm,1} \qquad (2\ a)$$

$$\frac{dY_{Xm,i}}{dt} = \alpha Y_{Xm,i-1} - \alpha Y_{Xm,I}\ ,\ i = 2,..,n \qquad (2\ b)$$

$$\frac{dM}{dt} = -\beta(X_m + Y_{Xm})M + \alpha r Y_{Xm,n} - \delta M \qquad (3)$$

The parasitemia, as percentage of infected RBCs, is calculated by summing over the parasite age-stages and dividing by the total number of RBCs:

$$Y_{Xm} = \sum_{i=1}^{n} Y_{XmIi} \qquad (4)$$

$$P = \frac{Y_{Xm}}{X_m + Y_{Xm}} 100 \qquad (5)$$

The initial number of infected RBCs is informed by the inoculum size, its viability ω and the mouse blood volume V_n.

$$Y_{Xm,0,i} = \omega \frac{inoculum}{Vn} \qquad (6)$$

For reference, population models for murine parasite growth and drug treatment were estimated via a maximum likelihood approach on trust region optimization.

Data, parasite growth and PKPD models in human VIS experiments

Data in VIS

Parameters for the parasite growth models were estimated using previously published (26) parasite growth data from 177 malaria-naïve healthy volunteers enrolled in 27 cohorts as part of 14 VIS studies. Briefly, volunteers were inoculated intravenously on Day 0 with human erythrocytes infected with *P. falciparum* (3D7 strain). Treatment commenced on day 7-9 after infection. Parasite growth was monitored using a quantitative PCR assay (*P. falciparum* 18S rRNA gene). Specifics of parasite growth monitoring and data processing can be found in (26).

Parameters for drug efficacy were estimated from parasite clearance data (Table S1) collected from volunteers administered single doses of OZ439 (artefenomel)(11) (Cohorts 4, 5, and 6) and MMV048 (Cohorts 15, 16, and 27) (20). In the MMV048 cohorts, gametocyte concentration data were also available, where parasite measurements were discarded if the gametocyte count exceeded 10% of the total parasite count. Further details of the data and clinical trial identifiers are given in Table S1. All data was previously published (11, 21). As previously reported, all studies were approved by the QIMR-B Human Research Ethics Committee and all subjects provided informed consent (26).

Pharmacokinetic models of OZ439 and MMV048 in VIS

Human Population pharmacokinetic (PK) modelling of the OZ439 and MMV048 concentration versus time profiles was performed using Monolix (Version Monolix 2018R1). A 2-compartment PK model with zero order absorption (Equation S1) best described MMV048 concentrations and a 2-compartment PK model with first order absorption described the OZ439 concentrations (Equation S2). Structural PK model specifications and individual parameter can be found in Supplementary File 1.

Mathematical models of within-host parasite growth and post-treatment parasite clearance in VIS

P. falciparum-human infection is described via difference equations able to capture the changing age-structure of the parasitemia over time. The difference equations for *model S* (Equations 7-9) and *model i* (Equations 10 and 11), with incorporated drug action as specified in the Results section are given below (Equations 7-11. We estimated parasite growth and treatment effects in a two-step sequential process. Firstly, parasite growth parameters were estimated from parasite growth data before treatment. Secondly, we fixed the individual posterior median of parasite growth parameters and individual PK parameters to estimate parameters of drug efficacy (Fig. 1a). Treatment effect E incorporates parasite death through treatment as an increase in parasite death rate δ_p. The evaluated treatment models include a direct drug effect model and additional drug induced growth retardation causing a lengthening of the parasite life cycle length α_l. Model

output of *model S* is the number of circulating parasites P_{circ} (Equation 14). The parasite multiplication factor *pmf* can be calculated for *model S* using the intrinsic parasite multiplication rate r_p and death rate δ_p. It constitutes an estimation of the average number of merozoites that emerge from one infected RBC after a reproduction cycle within an RBC has been finished and successfully invade new RBCs at parasite age a=1 has completed (Eq. 7). Details of the parameters are provided in Table 3.

Model S, mechanistic asexual parasite growth model incorporating parasite stages and drug effect:

Our mechanistic model of growth of parasite density P, over the life cycle of length a_L =39 hours, at age a and time t is given by:

$$P(a,t) = \begin{cases} P(a-1,t-1)e^{-\delta_p}, a = 2,3,\dots,a_l \\ r_p P(a_l,t-1)e^{-\delta_p}, a = 1 \end{cases} \quad (7)$$

The direct drug effect on this model is incorporated via E (Equation 12) representing the drug-concentration dependent increase of parasite death rate δ_p.

$$P(a,t) = \begin{cases} P(a-1,t-1)e^{-\delta_p - E}, a = 2,3,\dots,a_l \\ r_p P(a_l,t-1)e^{-\delta_p - E}, a = 1 \end{cases}. \quad (8)$$

The direct drug effect model is extended to include drug concentration dependent growth retardation.

$$P(a,t) = \begin{cases} P(a,t-1)k_{ret}\frac{\left(1-e^{-\delta_p - E - k_{ret}}\right)}{\delta_p + E + k_{ret}} + P(a-1,t-1)e^{-\delta_p - E - k_{ret}}, a = 2,3,\dots,a_l \\ P(a,t-1)k_{ret}\frac{\left(1-e^{-\delta_p - E - k_{ret}}\right)}{\delta_p + E + k_{ret}} + r_p P(a_l,t-1)e^{-\delta_p - E - k_{ret}}, a = 1 \end{cases}. \quad (9)$$

Model i, exponential parasite growth model incorporating drug effect:

Parasite growth for the exponential *model i* is modelled on the logarithmic scale with the initial parasite concentration P_0 and parasite growth rate p_{gr}.

$$\ln(P(t)) = P_0 + p_{gr}\, t. \quad (10)$$

Treatment is included by decreasing parasite growth rate:

$$\ln(P(t)) = P_0 + \int_0^t (p_{gr} - E). \quad (11)$$

Additional equations:

In both models, drug effect is given by E;

Antimicrobial Agents and Chemotherapy

$$E = \frac{E_{max}C^{\gamma}}{EC50^{\gamma}+C^{\gamma}}. \quad (12)$$

and growth retardation in mechanistic *model S* by k_{ret};

$$k_{ret} = \frac{k_{ret,max}C^{\gamma}}{EC50^{\gamma}+C^{\gamma}}. \quad (13)$$

The maximum possible parasite age stage prolongation is therefore given by ((1/1-$k_{ret,max}$ [h^{-1}]))-1[h]) x 60, where one hour is the original length of the age stage and 60 converts hours into minutes.

In model S, the number of circulating parasites is given by summing parasite concentration up to the parasite-age stage α_s after which parasites sequester

$$P_{circ}(t) = \sum_{a=1}^{a_s} P(a,t). \quad (14)$$

The parasite multiplication factor over one parasite life cycle with length a_l for *model S* is given by

$$pmf = r_p e^{-\delta_p a_l}. \quad (15)$$

The parasite growth rate p_{gr} of exponential growth *model i* results in a parasite multiplication factor of:

$$pmf = \exp(p_{gr}\, a_l). \quad (15)$$

Under the assumption of exponential parasite growth (*model i*), the minimum inhibitory concentration, where parasite replication equals zero can be calculated with

$$MIC = EC50 \left(\frac{p_{gr}}{E_{max}+p_{gr}}\right)^{\frac{1}{\gamma}}. \quad (16)$$

Parameter estimation

Parasite growth and pharmacodynamic parameters for humans were estimated in R (Version 3.6.0) with package RStan (Version 2.18.2(45)) using a Bayesian hierarchical modeling approach. In brief, this means that subject and/or trial dependent parameters were defined as a second hierarchy level in addition to the population parameters. Parameters were estimated using a non-centered parameterization approach (46) and then transformed using inverse logit transformation within pre-specified lower and upper bounds(47) based on biological background information (Table 3). Prior distributions for the population mean parameters were given by standard normal distributions before the logit transformation. Priors for the inter-individual variability were defined by the Cholesky factors of the correlation matrices using a Cholesky LKJ correlation distribution with shape parameter of 2 for efficiency and computational

stability(47). We ran five chains with 4000 iterations each of which 2000 were used as a burn-in. The posterior samples were cumulated over all chains to illustrate the joint and marginal posterior distributions in Fig. S7-S12. The 95% credible interval of each parameter is given by the 2.5% and 97.5% quantiles of the posterior distribution (Fig. S3-S6). The M3-method was used for dealing with parasite measurements below the lower limit of quantification of 111 p/mL.

Models were evaluated using the R-package bayesplot (Version 1.6.0) and loo (Version 2.1.0), and model selection was based on the Watanabe-Akaike information criterion (WAIC, (48)), and the effective sample size n_{eff} ,an estimate of the number of independent draws from the posterior distribution. n_{eff} was required to be over 0.1 for all parameters. Additionally, divergences in any of the chains was evaluated visually and the convergence criteria $\hat{R}$ was calculated (potential scale reduction statistic should be less than 1.05). Posterior predictive checks were performed to visually assess how well the model fits the parasitological data.

Model simulation and analysis: Parasite clearance

We used the well calibrated models to estimate efficacy index parasite clearance rate and $\log_{10}$ PRR_{48} for a range of drug doses and regimes in both murine and human testing systems (Fig. 1b: Parasite clearance analysis).

Simulation and subsequent analysis of murine *P. berghei*-NMRI and *P. falciparum*-SCID infection was executed in a pooled manner: one set of parameters was drawn and simulated over all doses for each experiment. Population parameter distributions are defined as a log-normal distribution LN(μ,0.2μ) with the previously estimated mean μ (see Table S5 for a summary)(15). The experimental parameters infectivity parameter β and initial percentage of human RBCs H_0 were drawn from the pool of estimated parameter values. Simulations were performed using R-package IQRtools (Version 0.9.999).

P. falciparum – human infection was simulated with parameter variability implemented on a trial and subject level. Within one trial subjects were allocated the subject-specific parameters i_{pl} and δ_p and shared the parasite related parameters μ_{ipl}, σ_{ipl} and r_p. Parameters were drawn from the estimated variance-covariance within the bounds specified for estimation (Table 3). Simulations were performed in R. Human PK parameters were fixed to population level parameters. Additional information on the simulations can be found in Table S4. Parameters not previously estimated were fixed to values previously reported (15, 26). Simulation results were processed to extract the parasite clearance rate as described in (49). Potential lag phases after treatment at the beginning of the clearance curve and tail phases at the end of the clearance curve are excluded from analysis as described in (49). The clearance rate is extracted from the clearance curve on the log scale using linear regression and corresponds to the slope of the parasite clearance curve.

Model simulation and analysis: sensitivity of parasite clearance to host-parasite and drug dynamics

A global sensitivity analysis was performed to assess the sensitivity of parasite clearance after treatment to the parameters describing drug action and parasite growth. We performed a global sensitivity analysis by decomposition of the variance of model output (in this case parasite clearance rate) via sobol analysis (50). Calculation of the first order indices and total effect indices for all model parameters allows assessment of individual and combined parameter contributions to the variance of parasite clearance rate across the whole parameter space (51). As sobol analysis is computationally intensive due to the required number of points across the input parameter space (n=200,000) and bootstrap replicates (n=1000), we reduced computational time needed to simulate the parasite-PK-PD models by training emulators of the original models. We thus trained a Gaussian process model on simulation output for each of the parasite-growth models and doses analyzed using R-packages *hetGP* (Version 1.1.2). We normalized input parameters and output to be between 0 and 1 due to the large differences in scales. The criterion for acceptance of our trained model wasout of sample prediction with a predictive accuracy of R^2 >0.97. The sensitivity analysis was performed using the function *soboljansen* in the R-packages *sensitivity* (Version 1.16.2) on the trained Gaussian-process model. Parameters contributing under 1% were excluded from further analysis. Remaining parameters were summarized into parameters of host, parasite, host-parasite, and drug dynamics for the visualization of results according to Table 2.

Data availability

The datasets analysed during the current study are available from the corresponding author on request and with permission of Medicines for Malaria Venture

6. References

1. WHO. 2019. World malaria report 2019. World Health Organization, Geneva.

2. Burrows JN, Duparc S, Gutteridge WE, Hooft van Huijsduijnen R, Kaszubska W, Macintyre F, Mazzuri S, Mohrle JJ, Wells TNC. 2017. New developments in anti-malarial target candidate and product profiles. Malar J, 2017/01/15 ed. 16:26.

3. Flannery EL, Chatterjee AK, Winzeler EA. 2013. Antimalarial drug discovery - approaches and progress towards new medicines. Nat Rev Microbiol, 2013/11/13 ed. 11:849–62.

4. Jiménez-Díaz MB, Viera S, Ibáñez J, Mulet T, Magán-Marchal N, Garuti H, Gómez V, Cortés-Gil L, Martínez A, Ferrer S, Fraile MT, Calderón F, Fernández E, Shultz LD, Leroy D, Wilson DM,

García-Bustos JF, Gamo FJ, Angulo-Barturen I. 2013. A new in vivo screening paradigm to accelerate antimalarial drug discovery. PLoS One 8:e66967.

5. Phillips MA, White KL, Kokkonda S, Deng X, White J, El Mazouni F, Marsh K, Tomchick DR, Manjalanagara K, Rudra KR, Wirjanata G, Noviyanti R, Price RN, Marfurt J, Shackleford DM, Chiu FCK, Campbell M, Jimenez-Diaz MB, Bazaga SF, Angulo-Barturen I, Martinez MS, Lafuente-Monasterio M, Kaminsky W, Silue K, Zeeman A-M, Kocken C, Leroy D, Blasco B, Rossignol E, Rueckle T, Matthews D, Burrows JN, Waterson D, Palmer MJ, Rathod PK, Charman SA. 2016. A triazolopyrimidine-based dihydroorotate dehydrogenase inhibitor with improved drug-like properties for treatment and prevention of malaria. ACS Infect Dis, 2016/10/04 ed. 2:945–957.

6. Angulo-Barturen I, Jimenez-Diaz MB, Mulet T, Rullas J, Herreros E, Ferrer S, Jimenez E, Mendoza A, Regadera J, Rosenthal PJ, Bathurst I, Pompliano DL, Gomez de las Heras F, Gargallo-Viola D. 2008. A murine model of falciparum-malaria by in vivo selection of competent strains in non-myelodepleted mice engrafted with human erythrocytes. PLoS One, 2008/05/22 ed. 3:e2252.

7. Jimenez-Diaz MB, Mulet T, Viera S, Gomez V, Garuti H, Ibanez J, Alvarez-Doval A, Shultz LD, Martinez A, Gargallo-Viola D, Angulo-Barturen I. 2009. Improved murine model of malaria using Plasmodium falciparum competent strains and non-myelodepleted NOD-scid IL2Rgammanull mice engrafted with human erythrocytes. Antimicrob Agents Chemother, 2009/07/15 ed. 53:4533–6.

8. McCarthy JS, Marquart L, Sekuloski S, Trenholme K, Elliott S, Griffin P. 2016. Linking murine and human Plasmodium falciparum challenge models in a translational path for antimalarial drug development. Antimicrob Agents Chemother 60.

9. McCarthy JS, Sekuloski S, Griffin PM, Elliott S, Douglas N, Peatey C, Rockett R, O'Rourke P, Marquart L, Hermsen C, Duparc S, Mohrle J, Trenholme KR, Humberstone AJ. 2011. A pilot

randomised trial of induced blood-stage Plasmodium falciparum infections in healthy volunteers for testing efficacy of new antimalarial drugs. PLoS One, 2011/09/03 ed. 6:e21914.

10. Krause A, Dingemanse J, Mathis A, Marquart L, Möhrle JJ, McCarthy JS. 2016. Pharmacokinetic/pharmacodynamic modelling of the antimalarial effect of Actelion-451840 in an induced blood stage malaria study in healthy subjects. Br J Clin Pharmacol 82:412–421.

11. McCarthy JS, Baker M, O'Rourke P, Marquart L, Griffin P, Huijsduijnen RH. 2016. Efficacy of OZ439 (artefenomel) against early Plasmodium falciparum blood-stage malaria infection in healthy volunteers. J Antimicrob Chemother 71.

12. McCarthy JS, Ruckle T, Djeriou E, Cantalloube C, Ter-Minassian D, Baker M, O'Rourke P, Griffin P, Marquart L, Hooft van Huijsduijnen R, Mohrle JJ. 2016. A Phase II pilot trial to evaluate safety and efficacy of ferroquine against early Plasmodium falciparum in an induced blood-stage malaria infection study. Malar J, 2016/09/15 ed. 15:469.

13. WHO. 2009. Methods for surveillance of antimalarial drug efficacy. World Health Organization, Geneva.

14. White NJ. 2017. Malaria parasite clearance. Malar J 16:88.

15. Burgert L, Rottmann M, Wittlin S, Gobeau N, Krause A, Dingemanse J, Möhrle JJ, Penny MA. 2020. Ensemble modeling highlights importance of understanding parasite-host behavior in preclinical antimalarial drug development. Sci Rep 10:4410.

16. Charman SA, Arbe-Barnes S, Bathurst IC, Brun R, Campbell M, Charman WN, Chiu FC, Chollet J, Craft JC, Creek DJ, Dong Y, Matile H, Maurer M, Morizzi J, Nguyen T, Papastogiannidis P, Scheurer C, Shackleford DM, Sriraghavan K, Stingelin L, Tang Y, Urwyler H, Wang X, White KL, Wittlin S, Zhou L, Vennerstrom JL. 2011. Synthetic ozonide drug candidate OZ439 offers new hope

for a single-dose cure of uncomplicated malaria. Proc Natl Acad Sci U S A, 2011/02/09 ed. 108:4400–5.

17. Phyo AP, Jittamala P, Nosten FH, Pukrittayakamee S, Imwong M, White NJ, Duparc S, Macintyre F, Baker M, Möhrle JJ. 2016. Antimalarial activity of artefenomel (OZ439), a novel synthetic antimalarial endoperoxide, in patients with Plasmodium falciparum and Plasmodium vivax malaria: an open-label phase 2 trial. Lancet Infect Dis 16:61–69.

18. Dong Y, Wang X, Kamaraj S, Bulbule VJ, Chiu FC, Chollet J, Dhanasekaran M, Hein CD, Papastogiannidis P, Morizzi J, Shackleford DM, Barker H, Ryan E, Scheurer C, Tang Y, Zhao Q, Zhou L, White KL, Urwyler H, Charman WN, Matile H, Wittlin S, Charman SA, Vennerstrom JL. 2017. Structure-activity relationship of the antimalarial ozonide artefenomel (OZ439). J Med Chem, 2017/01/05 ed. 60:2654–2668.

19. Paquet T, Le Manach C, Cabrera DG, Younis Y, Henrich PP, Abraham TS, Lee MCS, Basak R, Ghidelli-Disse S, Lafuente-Monasterio MJ, Bantscheff M, Ruecker A, Blagborough AM, Zakutansky SE, Zeeman AM, White KL, Shackleford DM, Mannila J, Morizzi J, Scheurer C, Angulo-Barturen I, Martinez MS, Ferrer S, Sanz LM, Gamo FJ, Reader J, Botha M, Dechering KJ, Sauerwein RW, Tungtaeng A, Vanachayangkul P, Lim CS, Burrows J, Witty MJ, Marsh KC, Bodenreider C, Rochford R, Solapure SM, Jimenez-Diaz MB, Wittlin S, Charman SA, Donini C, Campo B, Birkholtz LM, Hanson KK, Drewes G, Kocken CHM, Delves MJ, Leroy D, Fidock DA, Waterson D, Street LJ, Chibale K. 2017. Antimalarial efficacy of MMV390048, an inhibitor of Plasmodium phosphatidylinositol 4-kinase. Sci Transl Med, 2017/04/28 ed. 9:eaad9735.

20. Sinxadi P, Donini C, Johnstone H, Langdon G, Wiesner L, Allen E, Duparc S, Chalon S, McCarthy JS, Lorch U, Chibale K, Möhrle J, Barnes KI. 2020. Safety, tolerability, pharmacokinetics and antimalarial activity of the novel Plasmodium phosphatidylinositol 4-kinase inhibitor MMV390048 in healthy volunteers. Antimicrob Agents Chemother https://doi.org/10.1128/AAC.01896-19.

21. McCarthy JS, Donini C, Chalon S, Woodford J, Marquart L, Collins KA, Rozenberg FD, Fidock DA, Cherkaoui-Rbati MH, Gobeau N, Möhrle JJ. 2020. A Phase 1, Placebo-controlled, Randomized, Single Ascending Dose Study and a Volunteer Infection Study to Characterize the Safety, Pharmacokinetics, and Antimalarial Activity of the Plasmodium Phosphatidylinositol 4-Kinase Inhibitor MMV390048. Clin Infect Dis https://doi.org/10.1093/cid/ciaa368.

22. Bates I. 2017. 2 - Reference Ranges and Normal Values, p. 8–17. *In* Bain, BJ, Bates, I, Laffan, MA (eds.), Dacie and Lewis Practical Haematology (Twelfth Edition). Elsevier.

23. Cromer D, Evans KJ, Schofield L, Davenport MP. 2006. Preferential invasion of reticulocytes during late-stage Plasmodium berghei infection accounts for reduced circulating reticulocyte levels. Int J Parasitol 36:1389–1397.

24. Lamikanra AA, Brown D, Potocnik A, Casals-Pascual C, Langhorne J, Roberts DJ. 2007. Malarial anemia: of mice and men. Blood, 2007/03/08 ed. 110:18–28.

25. Khoury DS, Cromer D, Akter J, Sebina I, Elliott T, Thomas BS, Soon MSF, James KR, Best SE, Haque A, Davenport MP. 2017. Host-mediated impairment of parasite maturation during blood-stage Plasmodium infection. Proc Natl Acad Sci U S A, 2017/07/05 ed. 114:7701–7706.

26. Wockner LF, Hoffmann I, Webb L, Mordmuller B, Murphy SC, Kublin JG, O'Rourke P, McCarthy JS, Marquart L. 2019. Growth Rate of Plasmodium falciparum: Analysis of Parasite Growth Data from Malaria Volunteer Infection Studies. J Infect Dis, 2019/11/05 ed. https://doi.org/10.1093/infdis/jiz557.

27. Khoury DS, Aogo R, Randriafanomezantsoa-Radohery G, McCaw JM, Simpson JA, McCarthy JS, Haque A, Cromer D, Davenport MP. 2018. Within-host modeling of blood-stage malaria. Immunol Rev 285:168–193.

747 28. Zaloumis S, Humberstone A, Charman SA, Price RN, Moehrle J, Gamo-Benito J, McCaw J, Jamsen
748 KM, Smith K, Simpson JA. 2012. Assessing the utility of an anti-malarial pharmacokinetic-
749 pharmacodynamic model for aiding drug clinical development. Malar J, 2012/08/31 ed. 11:303.

750 29. Saralamba S, Pan-Ngum W, Maude RJ, Lee SJ, Tarning J, Lindegårdh N. 2011. Intrahost modeling
751 of artemisinin resistance in Plasmodium falciparum. Proc Natl Acad Sci U S A 108.

752 30. Zaloumis SG, Cao P, Dini S, Davenport MP, Cromer D, Khoury DS, Fowkes FJI, McCaw JM,
753 Simpson JA. 2018. In Silico Investigation of the Decline in Clinical Efficacy of Artemisinin
754 Combination Therapies Due to Increasing Artemisinin and Partner Drug Resistance. Antimicrob
755 Agents Chemother, 2018/09/27 ed. 62.

756 31. Dini S, Zaloumis S, Cao P, Price RN, Fowkes FJI, van der Pluijm RW, McCaw JM, Simpson JA.
757 2018. Investigating the Efficacy of Triple Artemisinin-Based Combination Therapies for Treating
758 Plasmodium falciparum Malaria Patients Using Mathematical Modeling. Antimicrob Agents
759 Chemother, 2018/08/29 ed. 62.

760 32. Cao P, Collins KA, Zaloumis S, Wattanakul T, Tarning J, Simpson JA, McCarthy J, McCaw JM.
761 2019. Modeling the dynamics of Plasmodium falciparum gametocytes in humans during malaria
762 infection. eLife 8:e49058.

763 33. Teuscher F, Gatton ML, Chen N, Peters J, Kyle DE, Cheng Q. 2010. Artemisinin-induced dormancy
764 in Plasmodium falciparum: duration, recovery rates, and implications in treatment failure. J Infect
765 Dis 202.

766 34. Fidock DA, Rosenthal PJ, Croft SL, Brun R, Nwaka S. 2004. Antimalarial drug discovery: efficacy
767 models for compound screening. Nat Rev Drug Discov, 2004/06/03 ed. 3:509–20.

768 35. Murray L, Stewart LB, Tarr SJ, Ahouidi AD, Diakite M, Amambua-Ngwa A, Conway DJ. 2017.
769 Multiplication rate variation in the human malaria parasite Plasmodium falciparum. Sci Rep,
770 2017/07/27 ed. 7:6436.

771 36. Chotivanich K, Udomsangpetch R, Simpson JA, Newton P, Pukrittayakamee S, Looareesuwan S,
772 White NJ. 2000. Parasite multiplication potential and the severity of falciparum malaria. J Infect Dis
773 181.

774 37. Greischar MA, Reece SE, Savill NJ, Mideo N. 2019. The Challenge of Quantifying Synchrony in
775 Malaria Parasites. Trends Parasitol 35:341–355.

776 38. Kingston HW, Ghose A, Plewes K, Ishioka H, Leopold SJ, Maude RJ, Paul S, Intharabut B, Silamut
777 K, Woodrow C, Day NPJ, Chotivanich K, Anstey NM, Hossain A, White NJ, Dondorp AM. 2017.
778 Disease Severity and Effective Parasite Multiplication Rate in Falciparum Malaria. Open Forum
779 Infect Dis 4:ofx169–ofx169.

780 39. Douglas AD, Andrews L, Draper SJ, Bojang K, Milligan P, Gilbert SC, Imoukhuede EB, Hill AV.
781 2011. Substantially reduced pre-patent parasite multiplication rates are associated with naturally
782 acquired immunity to Plasmodium falciparum. J Infect Dis, 2011/04/05 ed. 203:1337–40.

783 40. O'Flaherty K, Ataide R, Zaloumis SG, Ashley EA, Powell R, Feng G, Reiling L, Dondorp AM, Day
784 NP, Dhorda M, Fairhurst RM, Lim P, Amaratunga C, Pukrittayakamee S, Hien TT, Htut Y, Mayxay
785 M, Faiz MA, Beeson JG, Nosten F, Simpson JA, White NJ, Fowkes FJI. 2019. Contribution of
786 Functional Antimalarial Immunity to Measures of Parasite Clearance in Therapeutic Efficacy
787 Studies of Artemisinin Derivatives. J Infect Dis, 2019/05/11 ed. 220:1178–1187.

788 41. Rottmann M, Jonat B, Gumpp C, Dhingra SK, Giddins MJ, Yin X, Badolo L, Greco B, Fidock DA,
789 Oeuvray C, Spangenberg T. 2020. Preclinical Antimalarial Combination Study of M5717, a

Plasmodium falciparum Elongation Factor 2 Inhibitor, and Pyronaridine, a Hemozoin Formation Inhibitor. Antimicrob Agents Chemother 64.

42. McCarthy JS, Rückle T, Elliott SL, Ballard E, Collins KA, Marquart L, Griffin P, Chalon S, Möhrle JJ. 2019. A Single-Dose Combination Study with the Experimental Antimalarials Artefenomel and DSM265 To Determine Safety and Antimalarial Activity against Blood-Stage Plasmodium falciparum in Healthy Volunteers. Antimicrob Agents Chemother 64.

43. Desjardins RE, Canfield CJ, Haynes JD, Chulay JD. 1979. Quantitative assessment of antimalarial activity in vitro by a semiautomated microdilution technique. Antimicrob Agents Chemother 16:710–718.

44. Sanz LM, Crespo B, De-Cózar C, Ding XC, Llergo JL, Burrows JN, García-Bustos JF, Gamo F-J. 2012. P. falciparum In Vitro Killing Rates Allow to Discriminate between Different Antimalarial Mode-of-Action. PLOS ONE 7:e30949.

45. Stan Development Team. 2020. RStan: the R interface to Stan.

46. Papaspiliopoulos O, Roberts GO, Sköld M. 2007. A General Framework for the Parametrization of Hierarchical Models. Stat Sci 22:59–73.

47. Stan Development Team. 2018. Stan Modeling Language Users Guide and Reference Manual. 2.18.0.

48. Watanabe S. 2010. Asymptotic Equivalence of Bayes Cross Validation and Widely Applicable Information Criterion in Singular Learning Theory. J Mach Learn Res 11:3571–3594.

49. Flegg JA, Guerin PJ, White NJ, Stepniewska K. 2011. Standardizing the measurement of parasite clearance in falciparum malaria: the parasite clearance estimator. Malar J 10.

50. Sobol′ IM. 2001. Global sensitivity indices for nonlinear mathematical models and their Monte Carlo estimates. Math Comput Simul 55:271–280.

51. Zhang X, Trame M, Lesko L, Schmidt S. 2015. Sobol Sensitivity Analysis: A Tool to Guide the Development and Evaluation of Systems Pharmacology Models. CPT Pharmacomet Syst Pharmacol 4:69–79.

Figure 1: Standardized workflow for the systematic investigation of parasite-host-drug dynamics throughout the (pre)-clinical antimalarial development process. (a) Mechanistic models of parasite growth are calibrated to extensive undisturbed parasite growth (control) data in murine and human infection experiments on a population (mouse) or individual (human) level. Combined with models of drug-concentration (PK) over time, they are used to calibrate to treatment data over multiple doses and drugs. Models were selected for further analysis based on appropriate goodness of fit measures and assessment of biological plausibility. (b) Model simulation over multiple drugs and doses facilitates the comparison of the parasite reduction rate over all experimental systems. Subsequent sensitivity analysis allows the identification of parasite-, host-, or drug-dynamics as the drivers of experimental outcomes.

Figure 2: Experimental sampling design and investigated parasite-host dynamics in preclinical and clinical antimalarial drug development. Parasitemia of a typical subject in each experimental system is shown on the left side. Subjects are inoculated on day 0 (black syringe) and treatment (blue syringe, oral dose) commences on the same day or up to four days afterwards in murine malaria infection (a, b) and after seven to nine days in human infection (c). Each dot represents one measurement, with black dots indicating untreated growth/growth before treatment and blue dots representing parasitemia after treatment. Separate control groups were measured in murine experiments. The murine infections are measured in percent of infected RBCs P[%] (a, b), and human infections are measured in infected RBCs per mL P[p/mL] (c) (Table 1). For illustrative purposes, we added a conversion of P[p/mL] to P[%] in VIS (c) based on the assumption of $5x10^9$ RBCs/mL in male humans (22). The schematics of mathematical models used to describe parasite growth in the respective system are shown on the right side. In murine malaria infection (a, b), capturing uninfected (X) and infected (Y) RBCs dynamics is crucial to understand implications of resource limitation (*P. berghei*-NMRI infection) and resource replenishment (*P. falciparum*-SCID infection) (15). Details on murine model structure can be found in the Material and Methods, Equations 1-6. In contrast, low total numbers of parasites P(t) in *P. falciparum*-human infection and increased number of measurements shift modelling focus on dynamics of intra-erythrocytic parasite-stages over time (c). The exponential growth *model i*, can only be used to capture parasite growth of *P. falciparum* in SCID mouse and human as data are not informative enough in *P. berghei* – NMRI infection.

Figure 3: Population parasite growth prediction in VIS. Median parasite densities (black dots) with their 90-percentiles over the time starting four days after inoculation for the 177 subjects in VIS**(26)**. Model predictions show the median (red) and 90th percentile (blue) with credible intervals over 100 trials with 20 subjects. (**a**) The mechanistic growth *model S* captures parasite growth trends well over time with discrepancies between data and prediction being centered around parasitemia under the lower limit of quantification (LLOQ) of 111 p/mL and lower limit of detection of 10 p/mL (LLOD). We found a population posterior median (credible interval) of the initial parasite load (four days after infection) of 2.59 (2.44-2.74) [log(p/mL)], a median parasite age μ_{ipl} of 14.0 h (12.1 – 15.6) with a standard deviation σ_{ipl} of 4.32 h (3.83-4.90). The intrinsic parasite multiplication rate r_p of 55.2 (46.3 – 68.5) and death rate δ_p of 0.0302 (0.0263-0-0353) [1/h] describe the intra-erythrocytic replication dynamics of the parasite. (**b**) The exponential parasite growth in *model i* leads to linear growth behavior on the log-scale, so does not capture the oscillating parasite growth behavior. We estimated a growth rate r_p of 0.0649 [1/h] (0.0620-0.0678). The posterior predictive checks are illustrated in Fig. S7 (*model S*) and Fig. S8 (*model i*).

Figure 4: Population prediction after treatment with OZ439 in *P. falciparum*-human infection for mechanistic growth *model S* (a-c) and exponential *model i* (d-f). The simulated median (red) and 90th percentile (blue) with credible intervals over 100 trials with 20 subjects are compared to data of individual parasite densities (black dots) in the respective treatment group. For each treatment group, parasite clearance of a typical subject (Subject 1, 15 and 19) immediately after treatment is illustrated with individual predictions in the inset figures (for all subjects see Fig. S12 and Fig. S13). Immediately after treatment with 100 mg OZ439 **(a, d)** an increase in parasite densities, and transient decelerated parasite growth was observed which is captured by *model S* through the lengthening of the parasite life cycle. After treatment with higher doses **(b-c, e-f),** this effect is less influential, with more prominent parasite killing by the drug. After treatment with 500 mg **(c, f)** only four out of eight volunteers exhibited parasite recrudescence (see individual data in Fig. S5 and Fig. S6 and posterior distributions in Fig. S11 and S12). Vertical line (---) indicates time of treatment and the horizontal lines the LLOQ of 111 p/mL and LLOD of 10 p/mL.

Figure 5: Parasite clearance across the murine and human experiments after single dose treatment with OZ439. Within one experimental system the predicted clearance rates are fairly consistent. (a) *Model c* (*comp. erythr.*) of *P. berghei*-NMRI infection estimated a lower maximum drug effect E_{max} resulting in lower clearance rates (Table S5). (b) Compared to panel a and c, *P. falciparum*-SCID infection shows less variability. (c) The wide clearance range observed in model predictions of the exponential growth *model i* for *P. falciparum*-human infection stems from the wide posterior distribution of the maximum drug effect E_{max}. Parasite clearance rates were calculated from simulation output using the methodology provided in (49). For comparability a conversion to $\log_{10} PRR_{48}$ was added as secondary y-axis where $\log_{10} PRR_{48}=\log_{10}(e^{\text{parasite clearance rate x48}})$.

Figure 6: Exemplary results of the sensitivity analysis of parasite clearance after OZ439 treatment towards parameters of host, parasite, host-parasite, and drug dynamics for (a) *P. berghei* – NMRI , (b) *P. falciparum* – SCID, and (c) *P. falciparum*- human infection. Using sobol sensitivity analysis, first order effects measure individual parameter contributions and the total effect indices summarize individual and interactive parameter contributions to the outcome variance (see Material and Methods).

Table 1: Overview of the data and experimental outcomes in our analysis of murine and human malaria infection. Untreated parasite growth behavior was informed by a separate control group in murine experiments, and by parasite growth data before treatment commences in human infection. Experimental outcomes evolve over the preclinical and clinical stages with increasing data richness per subject over time from crude efficacy measures such as activity and parasite reduction to more detailed concentration effect relationships. Measures of parasite reduction (e.g. parasite clearance rate or proportional antimalarial activity) are frequently used to evaluate compounds throughout the clinical development stages (2). SD: single dose, DD: double dose, TD: triple dose, QD: quadruple dose.

	***P. berghei ANKA* in NMRI mice**	***P. falciparum* (3D7) in SCID mice**	***P. falciparum* (3D7) in human**
no. subjects			
Control (Separate)	215 (Y)	132 (Y)	177 (N)
MMV390048	65	50	20
OZ439	200	48	24
no. subjects/dose	3-10	1-2	6-8
no. dose levels			
MMV390048	7 SD, 5 QD	2 DD, 6 QD	3 SD
OZ439	14 SD, 3 TD	10 SD, 1 DD	3 SD
Min exp. length [d]	3-4 (up to 30)	8 (up to 31)	8 (up to 30)
Inoculum [iRBCs]	2×10^7	3.5×10^7	1800-2800 (viable parasites)
Total cure (no. mice)			
MMV048	4x3 mg/kg (3)	4x20 mg/kg (2)	1x80 mg (8)
OZ439	1x30 mg/kg (30)	1x100 mg/kg (2)	-
Outcomes	- Activity - Cure (Survival) (Parasite clearance)	- PKPD relationship - Parasite clearance - Cure	- PKPD relationship - Parasite clearance - Cure
Parasitemia output	Percentage of infected RBCs	Percentage of infected RBCs	Concentration of infected RBCs per mL

Table 2: Classification of model parameters into host, parasite, host-parasite and drug parameters. Parameters were classified based on their dependency on host and parasite variables states and induction through those variables. Detailed description of parameters for murine models of *P. berghei* – NMRI and *P. falciparum* – SCID infection can be found in (15). Details on parameters of *P. falciparum* – human infection can be found in Fig. 2 and Table 3.

	***P. berghei* – NMRI**	***P. falciparum* – *SCID***	***P. falciparum* – human**
Host		• Initial percentage of human RBCs H_o • Base death rate of all RBCs λ • Parameters of RBC density dependent RBC clearance χ_{max} and $k\chi_{50}$	• Parasite death rate at each time stage δ_p
Parasite	• Infectivity parameter β • Number of merozoites per inf. RBC r • Attraction of parasite to reticulocyte ε • Parasite inoculum viability ω	• Infectivity parameter β • Number of merozoites per inf. RBC r • Parasite inoculum viability ω • Exp. parasite growth rate r_p • Initial parasitemia P_0	• Intrinsic parasite multiplication rate r_p • Distribution parameters of the initial parasite density μ_{ipl} and σ_{ipl}
Host- Parasite	• Parameters of infection induced RBC clearance γ_{max} and $k\gamma_{50}$ • Conc. of inf. Mouse RBCs achieving 0.5 growth retardation effect $k_{l,50}$	• Parameters of infection induced RBC clearance γ_{max} and $k\gamma_{50}$ • Base clearance of inf. RBCs φ	• Initial parasite density i_{pl}
Drug	• Parameters of concentration-effect relationship E_{max}, EC_{50} • Clearance rate for damaged parasites Cl_Y • First order rate constant for biological intermediate k_R	• Parameters of concentration-effect relationship E_{max}, EC_{50} • Clearance rate for damaged parasites Cl_Y • First order rate constant for biological intermediate k_R	• Parameters of concentration-effect relationship E_{max}, EC_{50} • Growth retardation parameter k_{ret}

Antimicrobial Agents and Chemotherapy

889 **Table 3: Parameters of the parasite growth and treatment models.** The bounds for parameter estimation were set to include
890 all plausible values based on previously published models **(28, 30–32)**.

Parameter	Unit	Description	Bounds [lower, upper]
i_{pl}	[p/mL]	Parasite density four days after inoculation (log transformed)	[1, 15]
μ_{ipl}	[h]	Mean of the initial parasite age distribution	[5, 10]
σ_{ipl}	[h]	SD of the initial parasite age distribution	[2, 20]
δ_p	[1/h]	Drug independent parasite death rate	[0.001, 1]
r_p	[-]	Parasite replication rate	[40, 80]
α_l	[h]	Length of the parasite life cycle	fixed to 39 h
α_s	[h]	Sequestration age of asexual parasites	fixed to 25 h
pmf	[]	Parasite multiplication factor	-
EC_{50}	[mg/mL]	Drug concentration causing 50% of E_{max}	MMV048: [0.001, 0.8] OZ439: [1E-6, 0.1]
E_{max}	[1/h]	Maximum effect of the drug	[0.0001, 1]
γ	[]	Hill-coefficient, steepness of the C-E curve	-
k_{ret}	[1/h]	growth retardation due to drug treatment	-
$k_{ret,max}$	[1/h]	Maximum growth retardation	[0.0001, 1]

891

Antimicrobial Agents and Chemotherapy

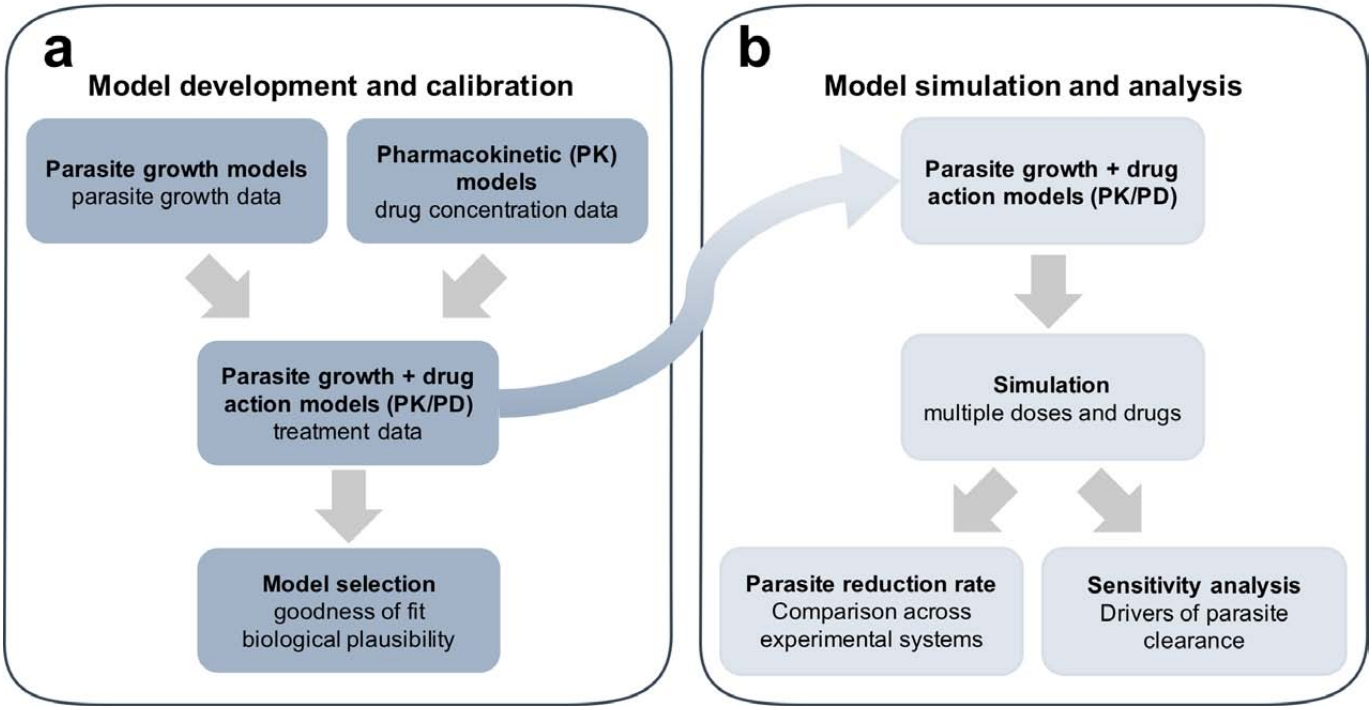

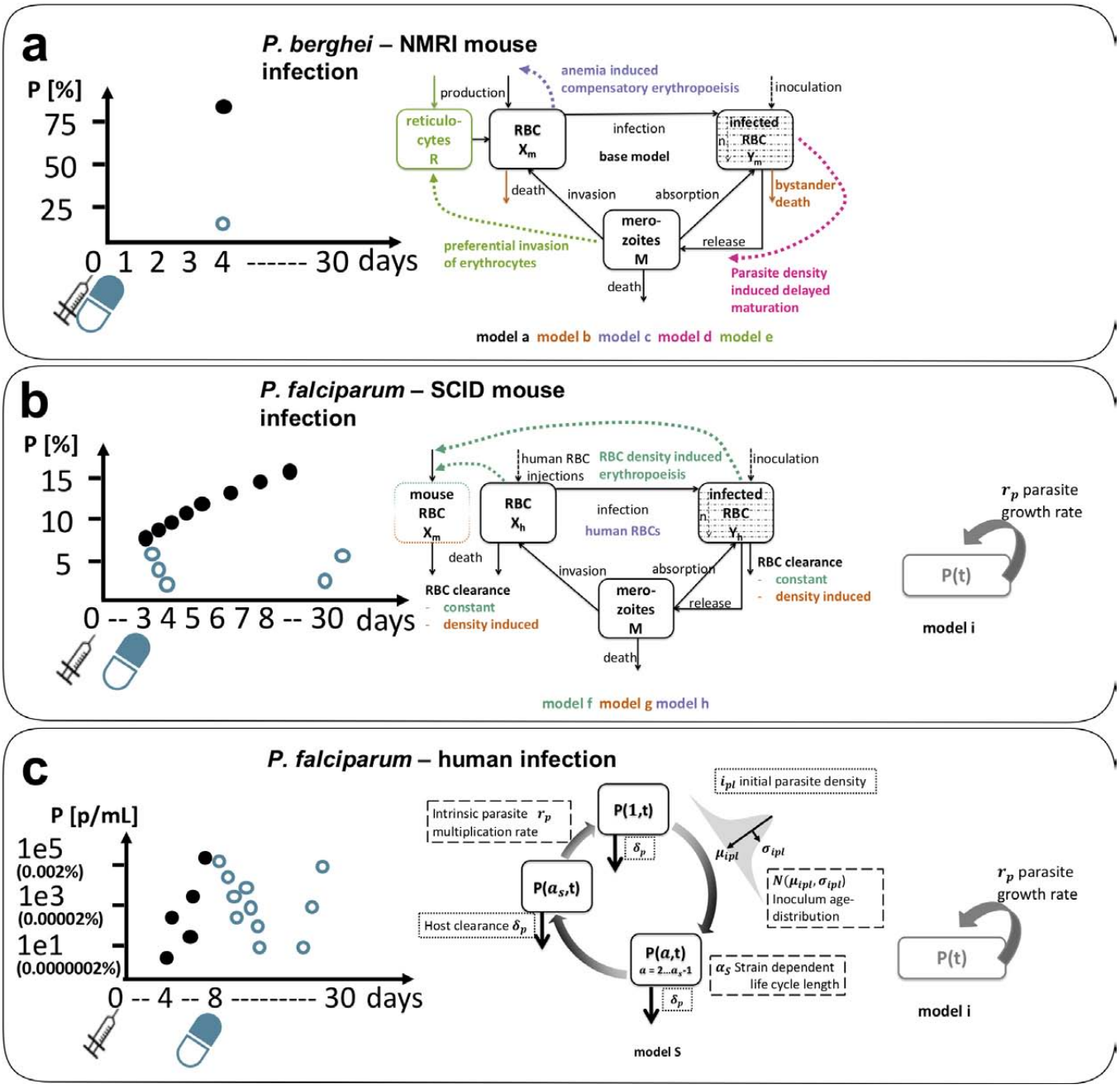

Antimicrobial Agents and Chemotherapy

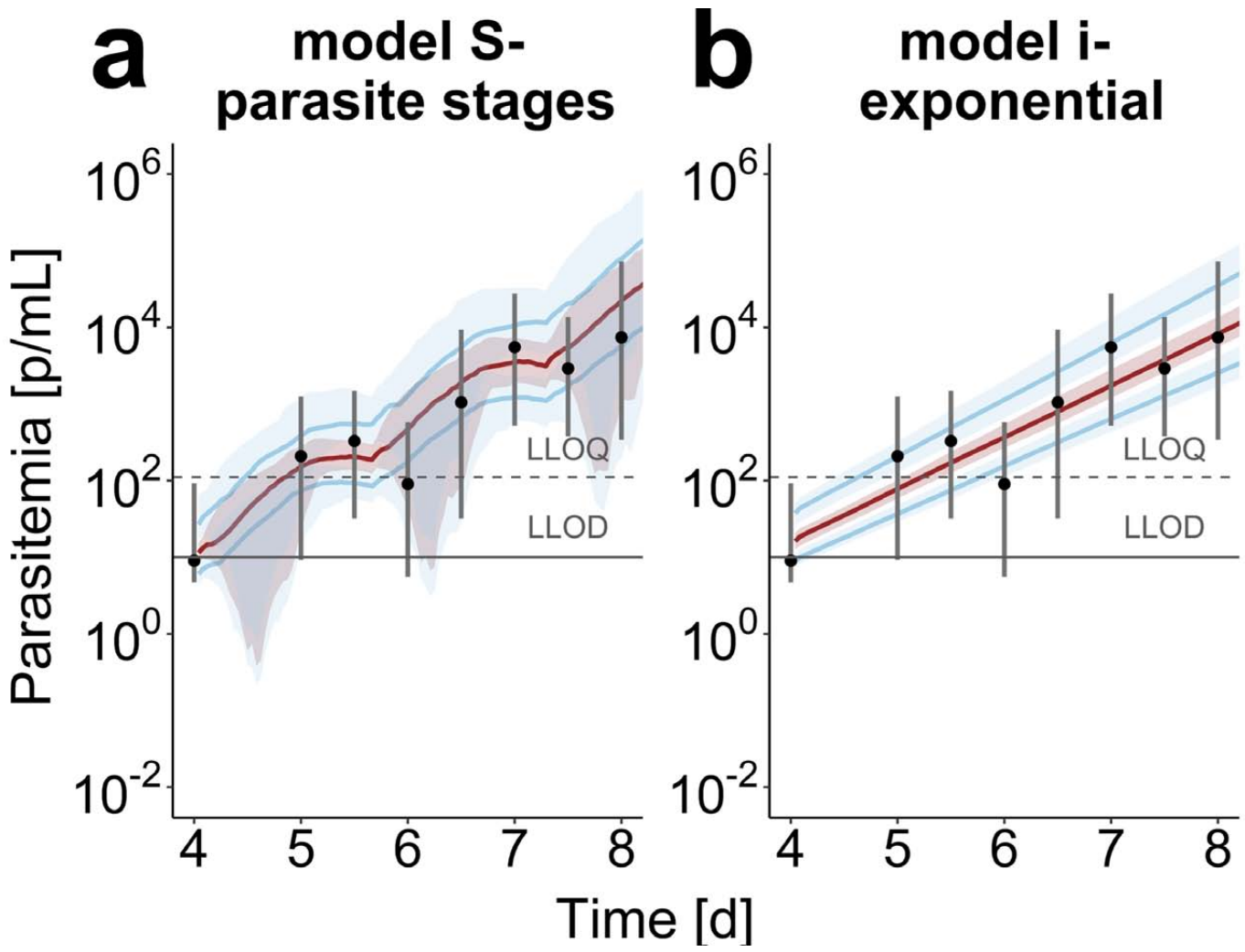

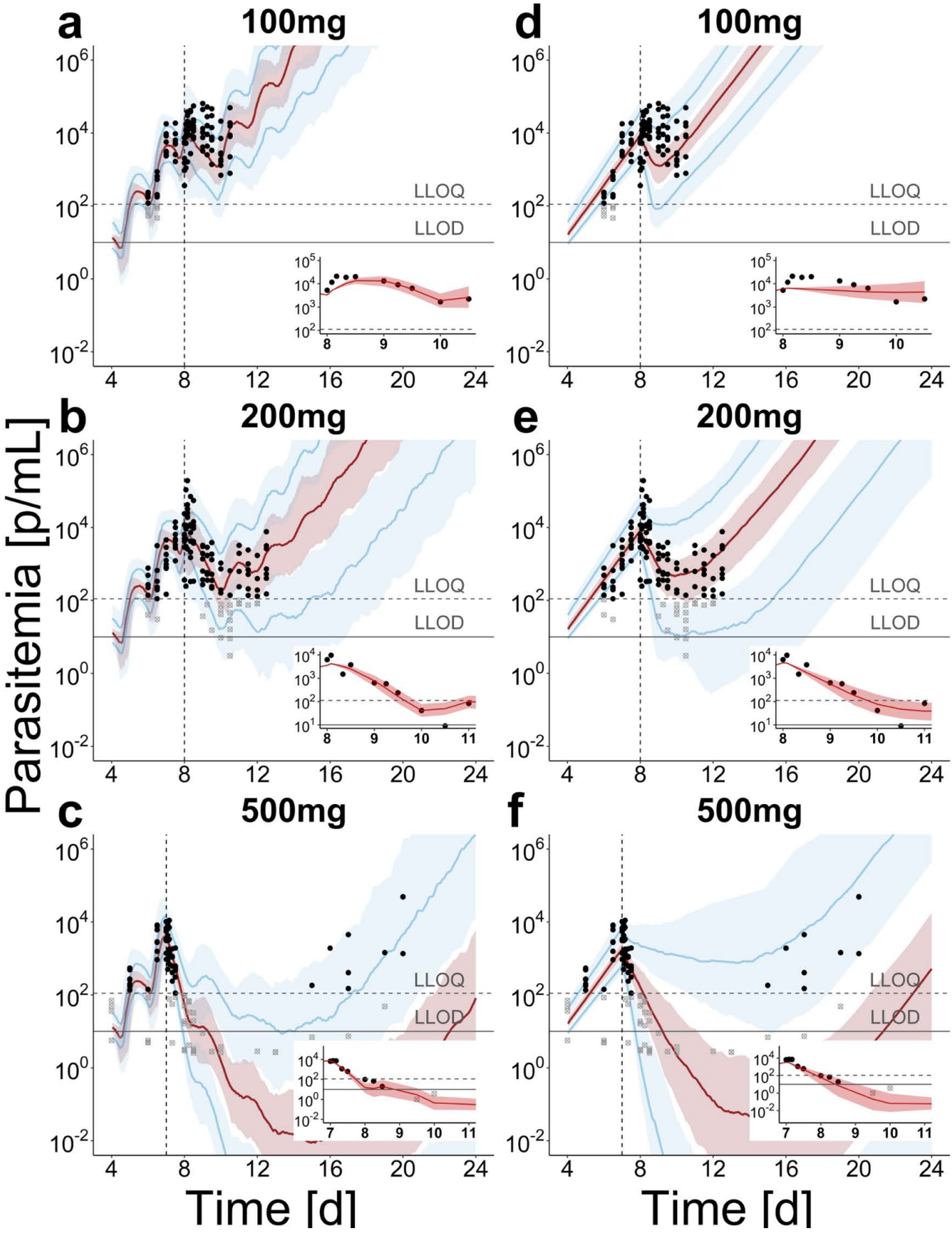

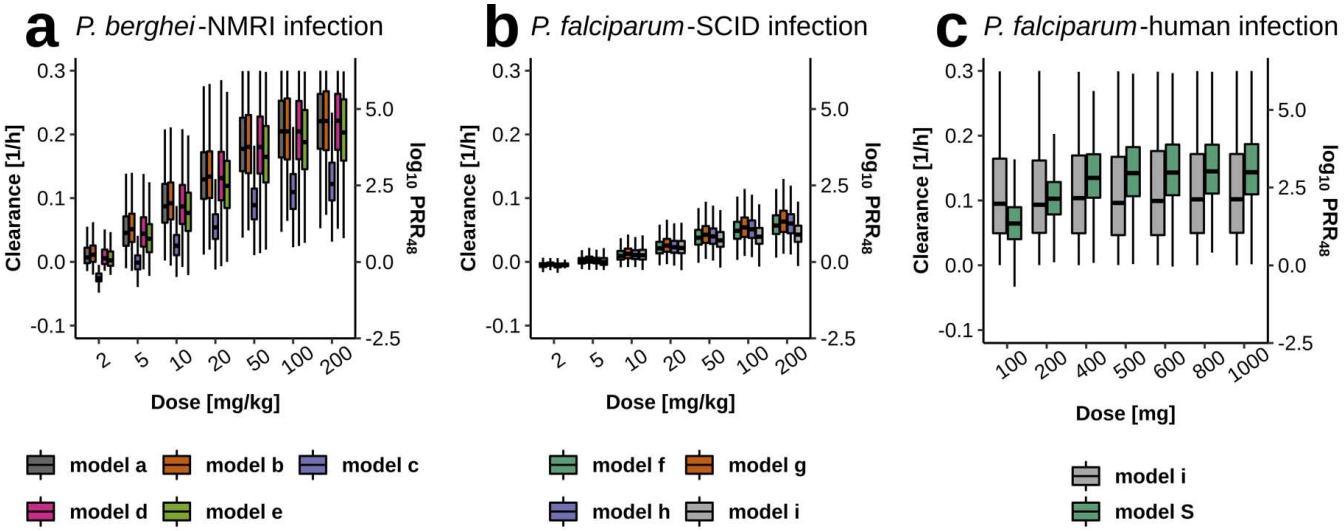

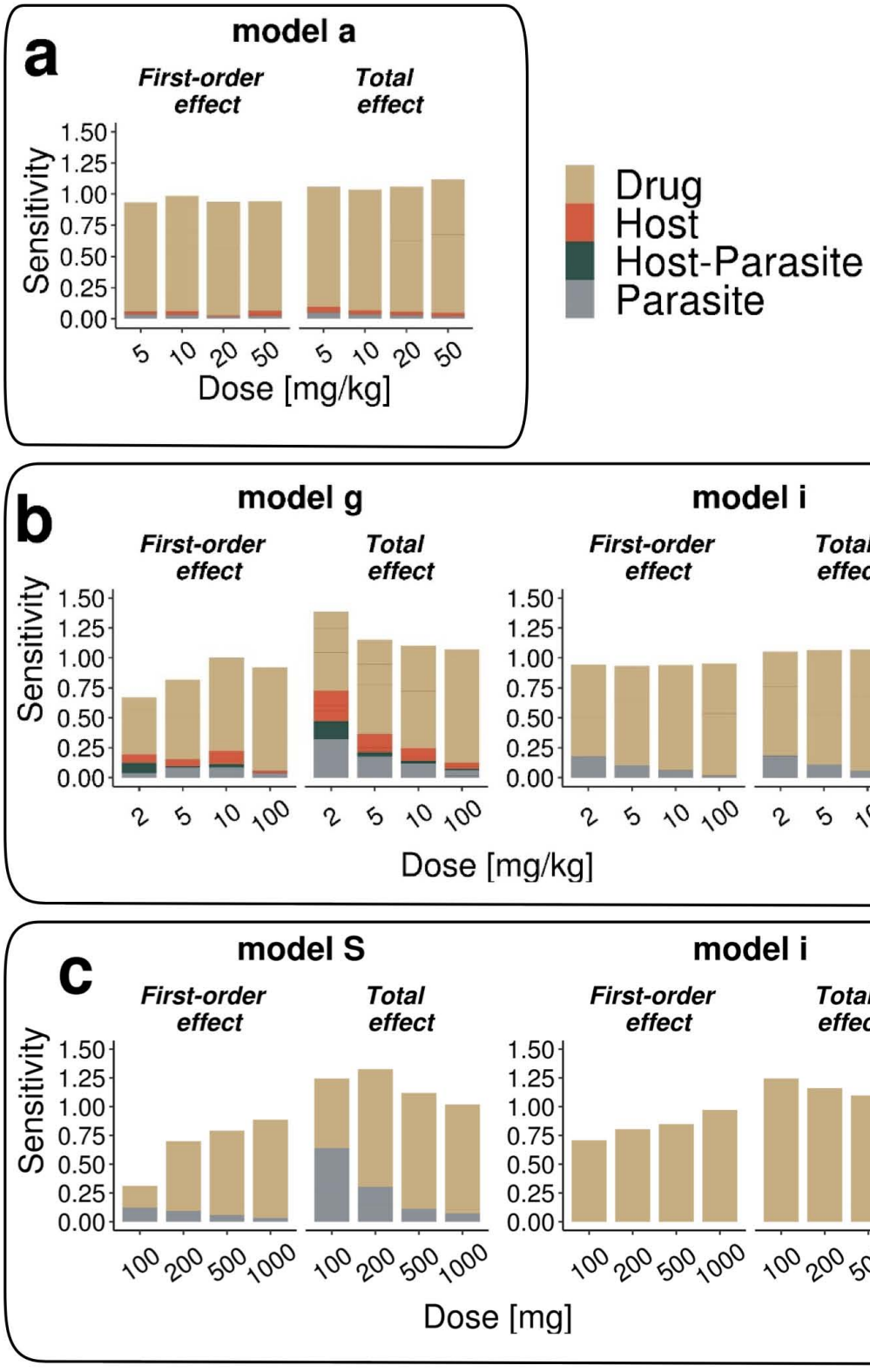

Author/s:
Burgert, L; Zaloumis, S; Dini, S; Marquart, L; Cao, P; Cherkaoui, M; Gobeau, N; McCarthy, J; Simpson, JA; Mohrle, JJ; Penny, MA

Title:
Parasite-Host Dynamics throughout Antimalarial Drug Development Stages Complicate the Translation of Parasite Clearance

Date:
2021-04-01

Citation:
Burgert, L., Zaloumis, S., Dini, S., Marquart, L., Cao, P., Cherkaoui, M., Gobeau, N., McCarthy, J., Simpson, J. A., Mohrle, J. J. & Penny, M. A. (2021). Parasite-Host Dynamics throughout Antimalarial Drug Development Stages Complicate the Translation of Parasite Clearance. ANTIMICROBIAL AGENTS AND CHEMOTHERAPY, 65 (4), https://doi.org/10.1128/AAC.01539-20.

Persistent Link:
http://hdl.handle.net/11343/273841

File Description:
Published version